

AERO-THERMAL INVESTIGATION OF END WALL AND SHOWERHEAD COOLING IN A NOZZLE VANE CASCADE

G. Barigozzi - P. Epis - A. Perdichizzi - S. Ravelli

Department of Engineering, University of Bergamo, Dalmine, Italy, giovanna.barigozzi@unibg.it,
paolo.epis@unibg.it, antonio.perdichizzi@unibg.it, silvia.ravelli@unibg.it

ABSTRACT

The aerodynamic and thermal performance of a gas turbine cascade with slot platform and vane showerhead cooling was investigated. The cascade was tested at a high inlet turbulence intensity level ($Tu_1 = 9\%$) and at variable cooling injection conditions of the upstream slot. Showerhead blowing ratio was maintained at the nominal value. Secondary flows and platform film cooling effectiveness measurements provided a comprehensive picture of the aerodynamic and thermal performance of the vane cascade. Slot cooling was found to slightly affect secondary flows. At small injection rates thermal coverage of the platform is limited to the front part, up to the passage vortex separation line, while for higher values a good thermal protection is obtained on the whole end wall surface. Showerhead injection contributes to cool the platform leading edge region and to reduce secondary losses.

NOMENCLATURE

$BR = \rho_c U_c / \rho_e U_e$	blowing ratio
c	blade chord
D	hole diameter
H	vane height
H_{12}	shape factor
l	length scale
m	mass flow rate
Ma	Mach number
$MFR = m_c / m_e$	coolant to mainstream mass
	flow ratio
$Re_{2,is} = U_{2,is} c / \nu$	isentropic outlet Reynolds
	number
s	vane pitch
Tu	turbulence intensity level
U	velocity
X, Y, Z	cascade coordinate system

α	injection angle
β	flow angle (tang. direction)
δ	boundary layer thickness
δ^*	displacement thickness
Λ_x	turbulence length scale
$\eta = (T_{aw} - T_e) / (T_c - T_e)$	adiabatic film cooling
	effectiveness
$\zeta = (U_{2,is}^2 - U_2^2) / \bar{U}_{2is,ms}^2$	energy loss coefficient

Subscripts

I	inlet
2	exit
ax	in axial direction
aw	adiabatic
c	cooling flow
e	free stream
is	isentropic condition
ms	at mid span

INTRODUCTION

High performance gas turbine engines operate at very high temperatures, requiring elaborate cooling systems to protect the exposed airfoil and end wall surfaces. In order to remove the excess heat from the exposed surfaces, conventional cooling involves full coverage film cooling of the airfoils and of the end wall, together with an effective internal convective cooling. In modern gas turbines, the first stage is highly loaded and the vane is characterized by high pitch-to-chord ratios also because of cooling requirements. Furthermore low aspect ratios are usually adopted. Both these features enhance the secondary flow intensity.

In modern gas turbines end wall cooling is typically accomplished both upstream of the vane leading edge, by exploiting the combustor to turbine interface gap purge flow (Oke and Simon

(2002), Thrift et al. (2011), and inside of the passage. In this region cooling air can be either discharged through the inter-platform gaps (Cardwell et al. (2006)) or through holes of different shape and position (Barigozzi et al. (2006)). It has been shown (see for example Friedrichs et al. (1996), Knost and Thole (2005), Nicklas (2001)) that the thermal protection capability of each specific cooling scheme strongly depends on the interaction between coolant and secondary flows, especially when coolant is injected in the vane front passage, upstream of the separation line. Thermal protection is also affected by the coolant to mainstream momentum ratio, governing the capability of the injected coolant to resist the horseshoe and passage vortices. From an aerodynamic point of view, Kost and Nicklas (2001) have shown that coolant injection performed through a slot located in the saddle point region has a strong impact on secondary flows, resulting in a horseshoe vortex intensification. The authors suggest to move the slot upstream in order to avoid this intensification, in the meanwhile reducing the influence of stagnation on coolant mass flow distribution along the slot. Shifting attention to the thermal point of view, Thole and Knost (2005) have shown that slot coolant injection at low blowing ratios (below 0.4) is not able to fully protect the whole end wall region, leaving the leading edge and the vane pressure side region almost uncooled. Conversely, Kost and Mullaert (2006) have shown that when coolant is injected with a higher blowing ratio of 0.62, the slot coolant is sufficient to cool the platform. They also confirmed that moving the slot upstream from the stagnation region allows to avoid the horseshoe vortex intensification.

When considering cascade geometries with different cooling systems, (for example with both vanes and platform cooled), the designer should also take into account what is called "phantom cooling". Not considering phantom cooling would lead to overestimation of surface metal temperature. According to Zhang et al. (2014), phantom cooling is a secondary effect: it consists in having some cooling benefits induced by coolant injected elsewhere. Examples of phantom cooling are cooling effects detected in an uncooled airfoil due to cooling of upstream lying vanes or blades. Another example is the ability of coolant injected on the pressure side of a vane to cool also a portion of the end wall or, conversely, the ability of slot platform coolant to protect the rear suction side. In this context, Zhang et al. (2014) have shown that properly orienting the pressure side and showerhead holes, a significant platform thermal protection can be achieved, especially when high momentum coolant is used.

In the last years Bergamo University has been involved, together with other Italian Universities, in a National Research Project (PRIN 2010/2011) entitled "Aerothermal investigation of cooled stage turbine: design optimization and experimental analysis (INSIDE)". Bergamo University task is focused on the experimental and numerical analysis of a nozzle vane cooling configuration with showerhead and platform slot cooling. The main goal of PRIN 2010/2011 is to evaluate the influence of hot streak migration across the passage on cooling performance. The present paper documents the first step of this research, i.e. the assessment of the aerodynamic and thermal performance of the cooled cascade with platform cooling, for variable injection conditions covering a blowing rate range from 0.4 up to 0.8. Uncooled (solid) cascade data are taken as reference.

EXPERIMENTAL DETAILS

The tunnel and the test models

Tests were performed in the subsonic wind tunnel for linear turbine cascades at the Turbomachinery Laboratory of Bergamo University. This is a continuously operating, suction-type wind tunnel (Fig. 1). The side walls were constructed of Plexiglas for optical



Fig. 1: View of the wind tunnel.

accessibility. A six-vane linear cascade was tested. A high loading profile (Zweifel coefficient of 1.18) typical of a first stage nozzle guide vane of a modern heavy duty Gas Turbine was experimentally investigated. The vane profile is characterized by a pitch to chord ratio of 1.04 and an aspect ratio of 0.69. The flow turning angle at design point is 73.5° . Details of cascade geometry are reported in Table 1.

The leading edge of the three central vanes is equipped with four staggered rows of cylindrical holes evenly distributed around the stagnation line (Fig. 2). Each row is composed of 16 cooling holes. Within each row, the hole-to-hole pitch is $5.9D$ and the hole length is $2.9D$. The diameter of the cooling holes D is 1.0 mm. Holes are spread over 90% of the blade height. The holes are angled at 90° to the surface. The choice of a normal injection angle in the present study was motivated by the need to share a unique showerhead geometry between partners having different points of view regarding internal and external cooling.

Platform cooling (Fig. 2) is accomplished by means of a rectangular slot located $0.54c_{ax}$ upstream of the leading edge plane, simulating the combustor to stator platform interface gap. The slot width w is $0.026c$ and extends over three passages. Coolant is discharged normally to the platform surface.

Table 1: Cascade geometry and operating conditions.

$c = 142.1 \text{ mm}$	$Ma_{2is} = 0.42$
$s/c = 1.04$	$Re_{2is} = 1.19 \cdot 10^6$
$H = 98 \text{ mm}$	$Tu_1 = 9 \%$
$H/c = 0.69$	$MFR_{slot} = 1.5 - 3.0 \%$
$\beta_1 = 90^\circ$	$BR_{slot} = 0.4 - 0.8$
$\beta_2 = 20^\circ$	$BR_{SH} = 3$

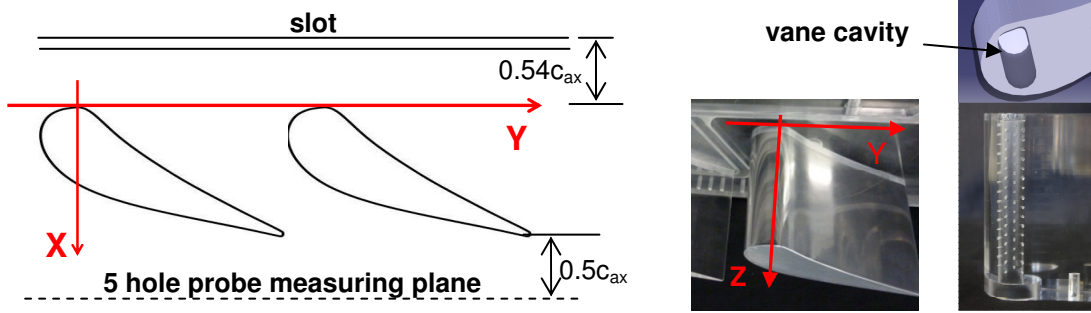


Fig. 2: Vane cascade geometry and cooled vane model.

Testing conditions and instrumentation

The cascade was tested at nominal expansion ratio, i.e. exit Mach number of $Ma_{2is} = 0.42$. The inlet turbulence intensity level was increased with respect to the free admission level (1.6%) by installing a grid of cylindrical rods in the wind tunnel inlet section. A 9% Tu_1 level at the vane leading edge plane was obtained by adopting 10 mm diameter rods and adjusting the distance of the grid from the cascade. Cascade operating conditions (Table 1) were controlled through a continuous monitoring of inlet total and static pressure and exit static pressure ($X/c_{ax} = 1.45$). Inlet total pressure and static pressure were measured by a three-hole probe in the admission section, about $1.6c_{ax}$ upstream of the cascade inlet plane. In the same location the inlet boundary layer (Fig. 3) and the turbulence intensity were also measured using a flattened Pitot tube and a hot-wire single wire probe (normal to the main flow direction). Tu_1 computation was thus based on stream wise rms velocity component. At that location a Tu_1 value of about 13% was measured. Tu_1 value at the leading edge plane (9%) was computed from a typical correlation for turbulence decay downstream of cylindrical rods. This value was confirmed by 2D LDV traverses performed at mid span section along the tangential direction 2 mm upstream of the leading edge plane. The numerical integration of the autocorrelation function of the acquired hot-wire signal yielded an integral length scale Λ_x of 11.8 mm. The uncooled vane profile pressure distribution (Fig. 4) was measured by an instrumented vane equipped with 39 wall taps, distributed along the vane mid span. Based on a 95% confidence interval, an uncertainty of $\pm 0.3\%$ for Tu_1 , of ± 0.001 for the profile Mach number and of $\pm 0.2 \text{ m/s}$ as a maximum for the inlet boundary layer velocity profile have been computed.

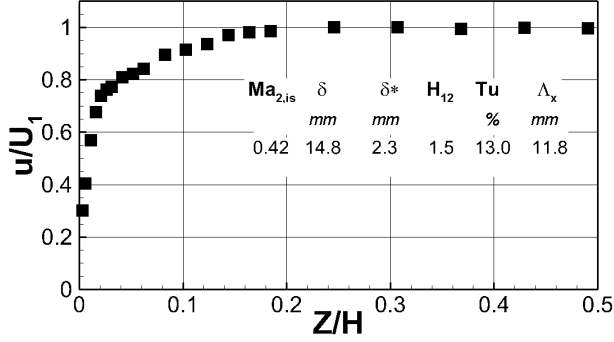


Fig. 3. Inlet boundary layer profile ($X/c_{ax} = - 1.6$).

Two secondary air supply systems were used to independently feed the cooled vanes and the slot. Mass flow ratios MFR up to about 3% and a constant blowing ratio BR of 3.0 were considered for platform and showerhead cooling respectively. The minimum MFR tested for the slot (1.5%) was selected in such a way to avoid mainstream ingestion inside the slot cavity. This condition was defined as the lowest tested MFR at which a TLC color change was detected along the whole slot tangential extension. Injection conditions were controlled by monitoring MFR , coolant total pressure and temperature inside the slot plenum and in the three vane feeding chambers as well. The injected mass flow was measured by orifice devices while coolant total pressure and temperature were measured by pressure taps and T-type thermocouples. A maximum variation of $\pm 0.15\%$ between the three vanes coolant total pressure assured a good flow sharing between the three cooled vanes. BR values were computed from MFR and coolant to mainstream area ratio.

The aerodynamic performance of the cascade was analyzed by means of oil&dye surface flow visualizations and secondary flows measurements. Traverses were performed in a plane at $X/c_{ax} = 1.5$ downstream of the trailing edge plane (see fig. 2), by using a 5-hole miniaturized aerodynamic pressure probe (1.6 mm conical head, advanced 50 mm to the stem). Measurement grid is made of 30 points per pitch in tangential direction times 15 points along the blade mid height. Grid spacing was reduced approaching the endwall surface: the first measurement point was 1.6 mm far from the wall. All flows were at room condition, resulting in a density ratio $DR = 1.0$. Cascade inlet total pressure and 5-hole probe data were used to compute kinetic energy loss coefficient ζ and deviation angle $\Delta\beta$. The computed uncertainty in the ζ value was $\pm 0.3\%$ at $\zeta = 3\%$ and $\pm 0.2\%$ at $\zeta = 30\%$, while in the flow angle it was $\pm 1^\circ$.

Platform film cooling effectiveness distributions were measured by means of wide banded Thermochromic Liquid Crystals (Hallcrest BM/R25C10WC17-10). TLC images were acquired by using a Nikon D7100 camera. Primary lighting system consists of two strips of white light LED. TLCs were first calibrated in situ, by replacing the cascade with an instrumented aluminium plate. This plate is heated on one side and cooled on the opposite side. The temperature gradient was captured by means of 10 T-type thermocouples installed just underneath the plate surface ($\pm 0.1^\circ\text{C}$).

Both calibration and measurements were performed in the dark, in order to eliminate any influence of background illumination. Moreover, an illumination intensity as uniform as possible was provided to the model surface by properly orienting the lighting system, while simultaneously avoiding any light reflection onto the camera. The light adjustment was performed with the vane model installed inside the test section and maintained also during calibration.

During tests the ambient temperature (about 25°C) was controlled in order to have a red platform surface colour as uniform as possible, i.e. at the lower bound of TLCs active band, with the wind tunnel running at the desired Mach number. The two cooling supply lines have been previously set at the desired mass flow rate and cooling air is heated up at about 37°C (resulting in a density ratio DR of about 0.95), but blowing in atmosphere. When a stable cooling temperature is

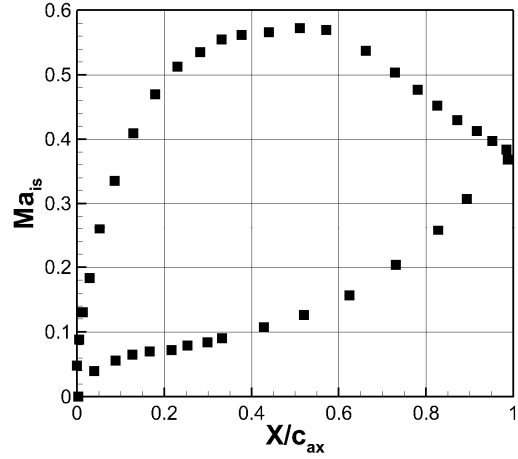


Fig. 4. Vane load (uncooled vane).

reached for each cooling flow as well as a red platform surface, the cooling lines are suddenly connected to the relative cascade cooling system (i.e. SH and slot). In the meantime camera starts acquiring images at a fixed rate of about 1 fps and temperature variation inside the two feeding chambers T_c and main flow temperature T_e are acquired as well for a test duration of 60s. RGB to hue conversion (Camci et al. (1992)) is applied to the image data recorded after a time period in the range between 30 s and 40 s, when a stable temperature level inside the plenum is reached as well as on the platform surface. The approach used in data processing is thus steady, but each test is run as a transient experiment, mostly to control conduction effects. The relatively large thickness (35 mm) of the end wall (Plexiglas made) assured to comply with wall adiabatic condition during test duration. Finally, a local averaging over a 5x5 pixel area was performed in order to reduce image size and noise. The resulting image size was 300 x 82 pixel, roughly corresponding to a spatial resolution of 1 mm x 1 mm. No further post processing techniques were applied to the recorded images. Film cooling effectiveness uncertainty depends on TLC ($\delta T_w = \pm 0.3^\circ\text{C}$) and thermocouple measurements ($\delta T_e = \pm 0.1^\circ\text{C}$ and $\delta T_c = \pm 0.5^\circ\text{C}$). η uncertainty will range from $\pm 4.2\%$ with $\eta = 0.8$, up to about $\pm 15\%$ when $\eta = 0.1$.

RESULTS AND DISCUSSION

Aerodynamic performance

Uncooled Cascade

Figure 5 reports the oil & dye surface flow visualization of the uncooled platform. The picture shows typical secondary flow traces, like the primary S_1 and secondary S_2 separation lines, associated with upstream boundary layer separation and horseshoe vortex separation from the endwall. The primary separation line S_1 extends up to $0.32c_{ax}$ upstream of the leading edge plane, i.e. it is far enough from the slot (located $0.54c_{ax}$ upstream of LE) so to not interact with coolant flow discharged along the slot. Downstream of S_2 it is also evident the pressure to suction side cross flow responsible for the buildup of tracing material on the vane suction side.

Figure 6 presents the distributions of kinetic energy loss coefficient ζ and secondary velocity vectors measured in the plane at $0.5c_{ax}$ downstream of the uncooled cascade. The typical vortex configuration of secondary flows can be observed. Most of the flow field is dominated by the passage vortex, as shown by the large region of high losses on the suction side of the wake, and by the secondary velocity vectors. The high pitch-to-chord ratio of the cascade

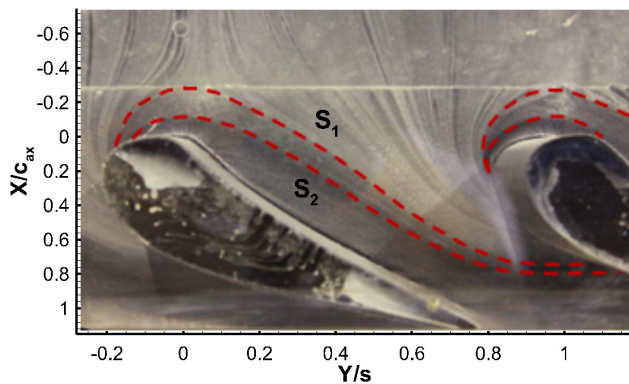


Fig. 5: Surface flow visualization of the uncooled platform.

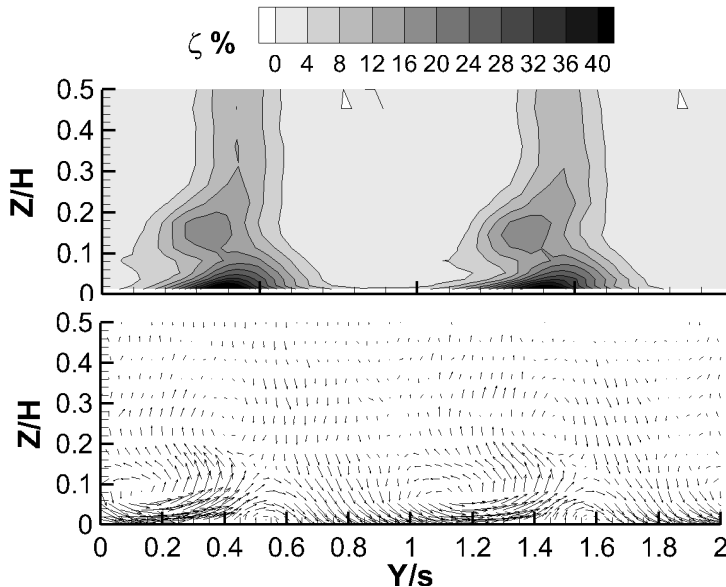


Fig. 6: ζ and secondary velocity vectors distributions (uncooled cascade).

contribute to increase passage vortex intensity (Perdichizzi and Dossena (1993)). Looking at the wake it can be observed that it is relatively thick and that the two dimensional region is limited to a narrow span around the mid span (from about $Z/H = 0.3$).

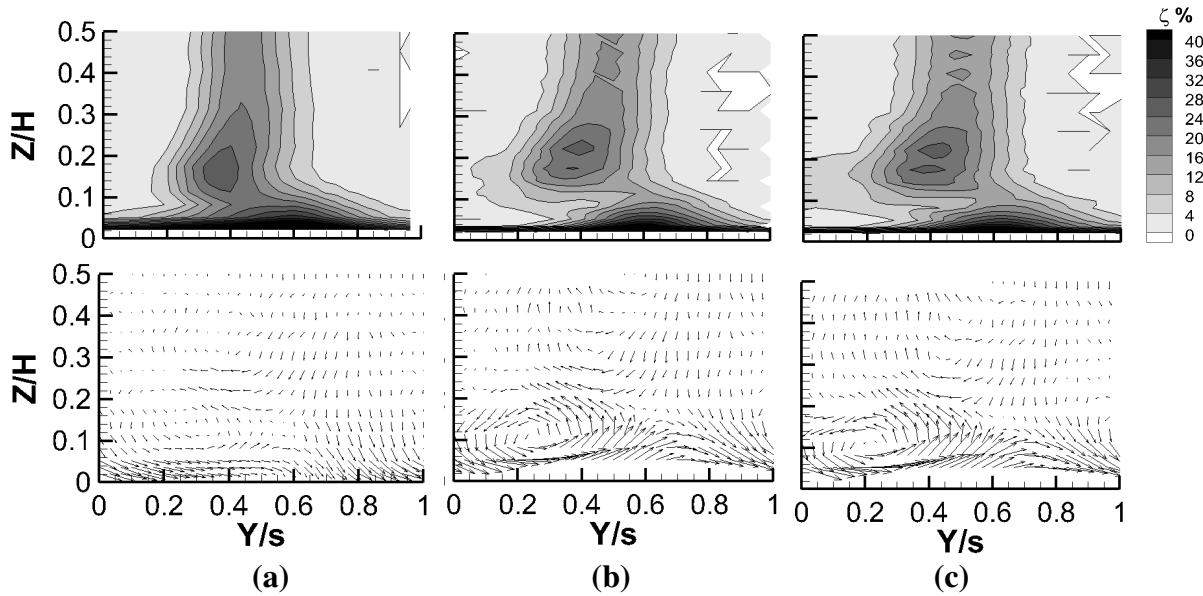


Fig. 7: ζ and secondary velocity vectors distributions ($BR_{SH} = 3.0$) for a) $MFR = 1.5\%$, b) $MFR = 2.0\%$ and c) $MFR = 3.0\%$.

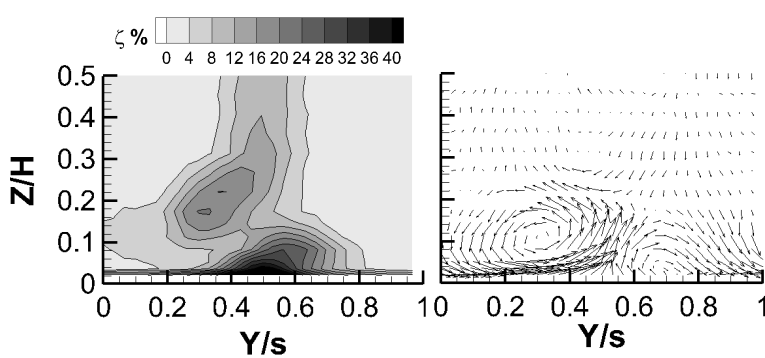


Fig. 8: ζ and secondary velocity vectors - SH off.

Cooled Cascade

Loss contour plots and secondary velocity vectors for the three tested slot MFR values (1.5% - 2.0% - 3.0%) and constant showerhead BR value (3.0) are shown in Fig. 7. If nominal injection condition results (Fig. 7b) are compared to the reference (uncooled) data (Fig. 6), the following modifications can be observed: (i) the wake loss strongly increases due to showerhead coolant injection, (ii) the

loss core associated with the passage vortex gets a higher peak value and widens, but its position does not change, (iii) the high loss region close to end wall is shifted towards the wake pressure side indicating a more intense end wall cross flow inside the passage. The result is a more twisted loss distribution along the span.

The passage vortex loss core reduces in pitch wise extension and moves closer to the end wall when slot MFR injection is reduced down to 1.5%. Conversely, a slot MFR increase up to 3.0% does not induce significant variations with respect to the case at slot MFR of 2.0%, but an enlargement of the loss region connected to the passage vortex.

In order to determine the separate contribution of slot and showerhead blowing to loss generation, a further test was carried out by replacing the cooled vanes (with showerhead holes) with the uncooled ones. The resulting loss distribution and secondary velocity vectors for slot injection at nominal condition ($MFR = 2.0\%$) are shown in Fig. 8. As expected, the wake loss returns to be similar to that one of the reference uncooled vane (see Fig. 6). Then, the absence of SH injection makes secondary flow effects related to the corner vortex to extend more towards the mid span (compare Figs. 7b and 8). To better appreciate differences between the investigated conditions, local data were mass averaged over the pitch, to obtain the spanwise distributions of deviation angle and losses. Secondary losses are defined as:

$$\bar{\zeta} = \frac{\overline{U}_{2is}^2 - \overline{U}_2^2}{\overline{U}_{2is,ms}^2} - \zeta_{ms} \quad (1)$$

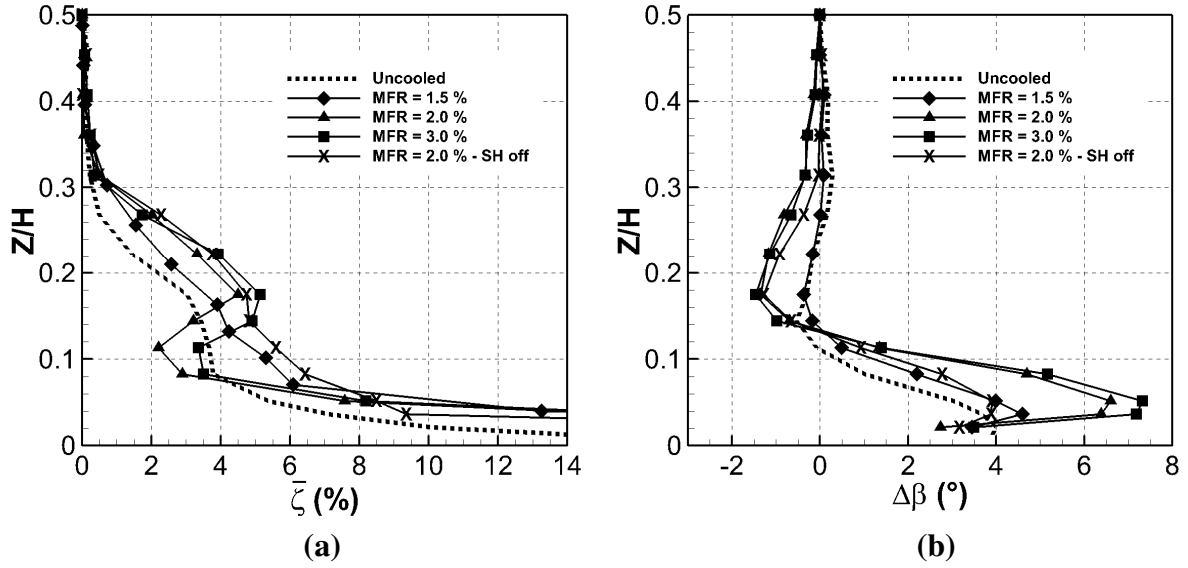


Fig. 9: Spanwise a) loss distribution and b) flow angle deviation.

Results are reported in Fig. 9. Slot injection confirms to be responsible for a relevant loss increase close to the platform, whatever the injection condition. Taking the uncooled vane case as a reference, a slot coolant injection at $MFR = 1.5\%$ results in a pitch averaged loss increase over the whole span region affected by secondary flows (i.e. up to $Z/H = 0.3$). Increasing the mass flow to the nominal value ($MFR = 2.0\%$), loss distribution takes a different shape, presenting a more defined loss core associated with the passage vortex. Increasing the injection rate up to $MFR = 3.0\%$, loss distribution is similar to that of $MFR = 2.0\%$ case, but the passage vortex related peak increases even more. A similar change in the loss distribution was shown by Sieverding (1985) in uncooled cascades: it was basically due to a passage vortex strengthening induced by a blade loading increase or by a strong thinning of the approaching boundary layer. Looking at the present case, a similar effect is produced by increasing the coolant flow rate injected through the slot located well upstream of the leading edge. But, when switching off showerhead cooling, the loss distribution comes back to the low MFR shape (i.e. with no trace of the passage vortex core), even if it remains on a high loss level in the region affected by passage vortex. Thus secondary flows modifications cannot simply be ascribed to a change in the inlet boundary layer. These results indicate that in the vane entrance region, i.e. just where horseshoe and passage vortices are forming, there is a strong and complex interaction between slot injection, showerhead injection and inlet boundary layer. The way this interaction takes place is complicated and not clear. Further research is required to explore issues that remain unclear.

The same general trend, confirming the higher intensity of the passage vortex with larger injection rates, can be deduced also looking at the deviation angle (Fig. 9b): when both slot and showerhead cooling are present, and slot is blowing with $MFR \geq 2.0\%$, higher underturning (lower $\Delta\beta$ values) as well as higher overturning are observed when compared to all the other cases. When instead slot blows at a low $MFR = 1.5\%$, only the overturning is slightly increased. Finally, when showerhead is switched off, overturning reduces back to the low MFR case, while underturning remains higher.

Figure 10 summarizes profile and secondary kinetic energy loss coefficients that were computed by mass averaging local loss distributions all over the passage. The so-called “thermodynamic” formulation (taking into account the coolant flow energy content) was used to compute an overall loss coefficient:

$$\zeta_{th} = \frac{\left(\overline{U_{2,is}^2} - \overline{U_2^2}\right) + \sum_{i=1}^2 MFR_i \left(U_{2,is,c,i}^2 - \overline{U_2^2}\right)}{(1 + MFR_{SH}) \overline{U_{2is,ms}^2}} \quad (2)$$

where $U_{2,is,c,i}$ is the velocity each coolant flow would have, assuming an isentropic expansion from supply plenum total pressure to the mass averaged static pressure measured $0.5c_{ax}$ downstream of the cascade, i.e. at measurement traverse location. This means that losses inside the supply systems are taken into account. Profile thermodynamic loss coefficients were computed in a similar way, but only considering showerhead coolant contribution:

$$\zeta_{th,ms} = \frac{\left(\overline{U_{2,is}^2} - \overline{U_2^2}\right) + MFR_{SH} \left(U_{2,is,SH}^2 - \overline{U_2^2}\right)}{(1 + MFR_{SH}) \overline{U_{2is,ms}^2}} \quad (3)$$

Secondary loss coefficient was then calculated by subtracting this profile loss to the overall one. Showerhead blowing is responsible for a huge increase in the profile loss coefficient, that increases from about 2.4-2.5 % for the uncooled case, up to 6.0 % for the cooled one. Profile loss coefficient is marginally affected by slot mass flow variation at constant showerhead blowing.

For low injection rates, i.e. up to $MFR < 2.0$, secondary losses do not significantly vary with MFR , remaining slightly larger than the uncooled reference case (+0.5 %). Secondary losses start increasing if slot mass flow rate exceeds 2.0%: at the largest tested MFR of 3.0% the secondary loss coefficient grows up to about 3.0 %. It is interesting to note that a similar increase in secondary losses takes place when showerhead is switched off, thus showing that showerhead injection reduces the secondary loss generation.

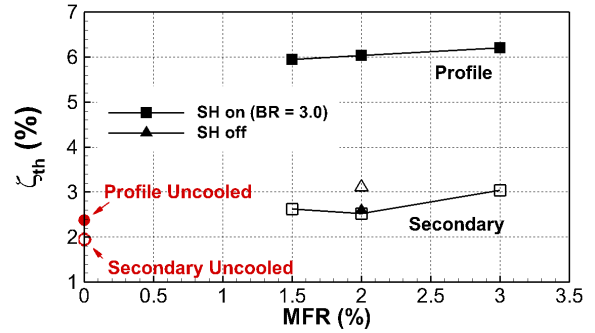


Fig. 10: ζ_{th} distribution.

Film cooling effectiveness

The performance of the cooling scheme was evaluated by examining the surface adiabatic effectiveness distributions on the platform. Figure 11 reports the effectiveness distributions for the three tested slot injection conditions ($MFR = 1.5\%$, 2.0% and 3.0%) at a fixed showerhead blowing ($BR = 3.0$). Note that the vane depicted in the figures with dotted lines indicates the real position of the vane (footprint) on the end wall. Also note that, due to perspective effects, the platform region close to the first vane suction side (the one with the leading edge at $Y/s = 0.0$) is shadowed by the vane itself. Moreover, it has to be noted that the two presented vane passages are not exactly the same. This is due to the fact that slot ends up just in front of the leading edge of the preceding vane (located at negative Y/s), thus affecting the horseshoe vortex formation and its migration towards the suction side of the following vane.

According to the literature, increasing the coolant mass flow always results in a better thermal protection. For a low coolant injection rate ($MFR = 1.5\%$ corresponding to a $BR_{slot} = 0.4$), coolant flow exiting the slot (Fig. 11a) is uniform enough in pitch wise direction to provide a satisfactory platform protection in the first zone downstream of the slot and in the middle of the passage; nevertheless, the region around the leading edge remains uncooled. This is due to the action of the horseshoe vortex legs that contribute to sweep coolant away from the platform leaving the surface around the leading edge practically uncooled both on the suction and pressure side. Anyway, a certain thermal coverage in the stagnation region is assured by showerhead flow. In fact, the coolant ejected from the holes located close to the platform is diverted towards the platform by the roll-up of horseshoe vortex legs. Test results with and without showerhead blowing (Fig. 12) show clearly the beneficial effect on the platform due to showerhead coolant. In fact, the leading edge region remains totally uncooled without showerhead blowing.

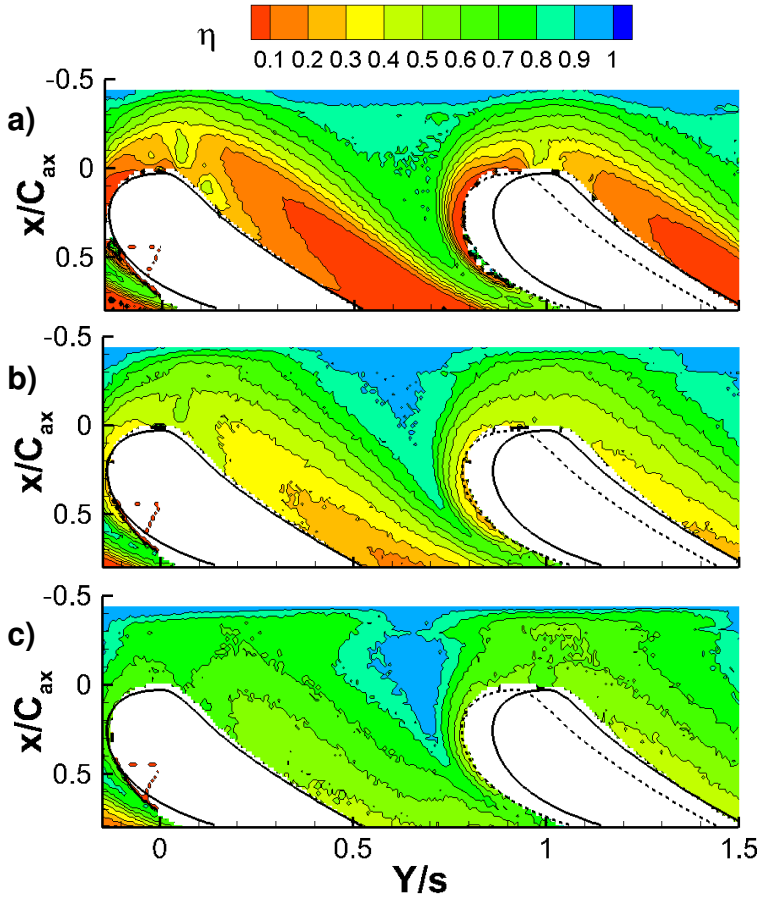


Fig. 11: Platform film cooling effectiveness distributions ($BR_{SH} = 3.0$): a) $MFR = 1.5\%$, b) $MFR = 2.0\%$ and c) $MFR = 3.0\%$.

passage (at $X/c_{ax} = 0.72$). In this condition coolant mass flow is high enough to resist to secondary flow action, thus assuring a thin coolant layer even downstream of the passage vortex separation line.

Figure 13 reports laterally averaged film cooling effectiveness η_{av} evaluated at different axial positions, for all the investigated slot injection conditions. Results have been obtained averaging over one pitch, i.e. between $Y/s = 0$ and 1.0 . Just downstream of the slot, where vane stagnation effect is marginal, all curves follow the same trend. As soon as the primary separation line is reached (S_1 line at $X/c_{ax} = -0.32$ - see Fig. 5) curves behave differently, showing a decreasing trend whose rate depends on the injection condition. The discontinuity at $X/c_{ax} = 0$ is related to the presence of vanes. According with the previous analysis, η_{av} progressively increases with

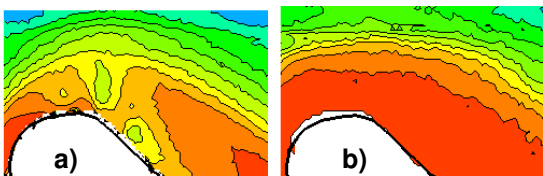


Fig. 12: Influence of showerhead: a) with and b) without ($MFR = 1.5\%$).

Within the passage, coolant persistency is good enough in the central region, so to allow coolant to reach the suction side of the vane, but downstream of the passage vortex separation line (see Fig. 5), effectiveness suddenly decays as coolant is totally entrained into the passage vortex.

Increasing MFR to 2.0% (corresponding to $BR_{slot} = 0.53$), thermal protection strongly improves: coolant is able to protect both sides of the leading edge region, even though η quickly decays moving downstream on the pressure side. Passage vortex and end wall cross flow from pressure to suction side are still able to wash out the coolant from the platform inside of the passage, driving the coolant towards the suction side. Showerhead injection still plays a role in cooling the leading edge region.

A further MFR increase up to 3.0% results in a very good thermal protection all over the platform with η levels above 0.5 rear in the

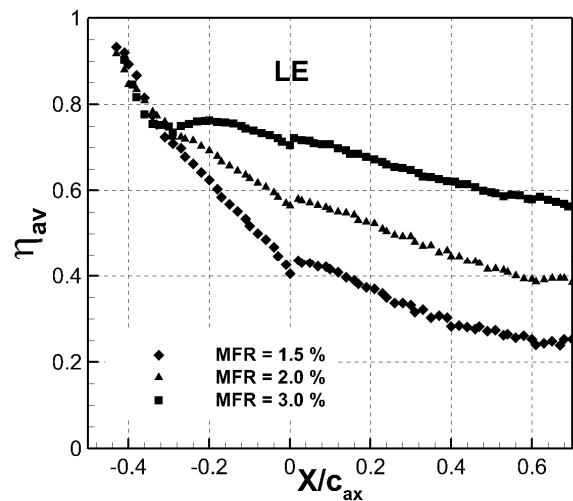


Fig. 13: Laterally averaged η .

rising MFR . At the highest investigated MFR of 3.0 %, the pitch averaged effectiveness at $X/c_{ax} = 0.7$ is above 0.55, reducing down to 0.4 and 0.23, for $MFR = 2.0$ % and 1.5 %, respectively.

Finally, an overall film cooling effectiveness was calculated by averaging the local values all over the platform surface up to $X/c_{ax} = 0.7$ (Fig. 14). These values define the global capability of the slot flow to protect the vane platform. An increase in coolant flow rate causes an almost proportional improvement of the area averaged film cooling effectiveness over the whole range of tested MFR values.

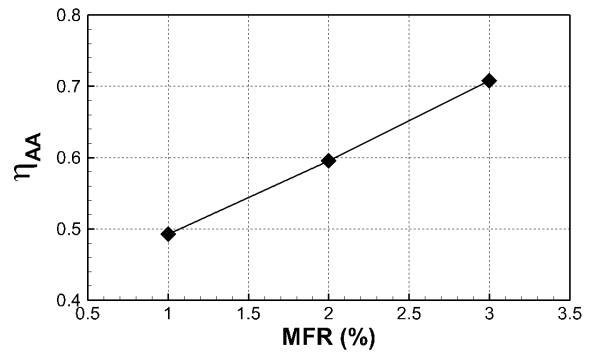


Fig. 14: Area averaged η .

CONCLUSIONS

A complete aerodynamic and thermal characterization of a nozzle vane cascade with showerhead and platform slot cooling was carried out at high inlet turbulence ($Tu_1 = 9.0$ %), with varying slot coolant mass flow ratio. The analysis was focused on platform cooling, so showerhead blowing was set at constant, nominal BR . Platform slot cooling, especially at the largest tested MFR , significantly affects the secondary flows structures and losses (+0.5%) but showerhead blowing has a much more relevant impact on profile loss augmentation (+3.5%). Film cooling effectiveness data showed a continuous increase in end wall thermal protection with rising MFR , up to reach a satisfactory coverage of the whole platform for $MFR = 3.0$ %. Finally, showerhead cooling through radial holes was found to provide a contribution to thermal coverage over one of the most critical regions to be cooled, i.e. the platform region around the leading edge. This coolant ejection somewhat interacts with the upcoming boundary layer, resulting in a modification of secondary flows. Further investigations are required to better understand the way this showerhead coolant interacts with the upcoming flow, the latter resulting from the mixing between the slot coolant and the mainstream.

ACKNOWLEDGEMENTS

This work has been founded by the Italian Ministry of Instruction, University and Research (MIUR) in the frame of PRIN 2010/2011 research project "Aerothermal investigation of cooled stage turbine: design optimization and experimental analysis".

REFERENCES

- Barigozzi G., Benzoni G., Franchini G., Perdichizzi A., 2006, *Fan-shaped Hole Effects on the Aero-Thermal Performance of a Film Cooled Endwall*, J. Turbomach. 128, 43-52.
- Camci C., Kim K., Hippensteele S.A., 1992, *A New Hue Capturing Technique for the Quantitative Interpretation of Liquid Crystal Images Used in Convective Heat Transfer Studies*, J. Turbomach. 114, 765-775.
- Cardwell N. D., Sundaram N., Thole K. A., 2006, *Effects of Roughness and Mid-Passage Gap on Endwall Film-Cooling*, J. Turbomach. 128, 62-70.
- Friedrichs S., Hodson H.P. Dawes W.N., 1996, *Distribution of Film-Cooling Effectiveness on a Turbine Endwall Measured with the Ammonia and Diazo Technique*, J. Turbomach. 118, 613-621.
- Knost D.G. and Thole K.A., 2005, *Adiabatic Effectiveness Measurements of Endwall Film-Cooling for a First Stage Vane*, J. Turbomach. 127, 297-305.
- Kost F. and Nicklas M., 2001, *Film-Cooled Turbine Endwall in a Transonic Flow Field: Part I – Aero-dynamic Measurements*, ASME paper 2001-GT-0145.
- Kost F. and Mullaert A., 2006, *Migration of Film-Coolant from Slot and Hole Ejection at a Turbine Vane Endwall*, ASME paper GT2006-90355.
- Nicklas M., 2001, *Film-Cooled Turbine Endwall in a Transonic Flow Field: Part II – Heat*

Transfer and Film-Cooling Effectiveness, ASME Paper 2001-GT-0146.

Oke R.A. and Simon T.W., 2002, *Film Cooling Experiments with Flow Introduced upstream of a First Stage Nozzle Guide Vane through Slots of Various Geometries*, ASME paper GT-2002-30169.

Sieverding C.H., 1985, *Secondary Flows in Straight and Annular Turbine Cascades*, In "Thermodynamics and Fluid Mechanics of Turbomachinery", NATO ASI Series E, No 97A, Vol. 1, 621-664 (VKI PP 1984-14).

Thole K.A. and Knost D.G., 2005, *Heat Transfer and Film-Cooling for the Endwall of a First Stage Turbine Vane*, Int. J. Heat and Mass Transfer 48, 5255-5269.

Thrift A. A., Thole K. A., Hada S., 2011, *Effects of Orientation and Position of the Combustor-Turbine Interface on the Cooling of a Vane Endwall*, ASME paper GT2011-45507.

Zhang L., Yin J. and Moon H.K., 2014, *The Effects of Vane Showerhead Injection Angle and Film Compound Angle on Nozzle Endwall Cooling (Phantom Cooling)*, ASME paper GT2014-25289.